

Determination of the Strong Coupling Constant with Jet Data

Junwu Huang*

*School of Physics, Peking University, China and
H1 Group, MPI Munich, Germany*

Supervisors: Dr. G. Grindhammer,[†] D. Britzger,[‡] and R. Kogler[§]

H1 Group, MPI Munich, Germany

(Dated: September 10, 2011)

Abstract

We fit the strong coupling constant α_s with ZEUS Inclusive-Jet and Dijet data in neutral current (NC) deep-inelastic scattering (DIS) at $Q^2 > 125\text{GeV}^2$. We managed to reproduce the Inclusive-Jet α_s fit result published by ZEUS Collaboration with the program we set up. With the Dijet data published by ZEUS Collaboration, we determined the α_s value to be $\alpha_s = 0.1173 \pm 0.0026(Stat)^{+0.0009}_{-0.0002}(PDF)^{+0.0103}_{-0.0097}(Theo)$. We also studied the α_s dependence on the renormalisation scale μ_R , the factorisation scale μ_F and parton distribution function(PDF) and justified the scales and PDFs we are using in the present project.

*Electronic address: curlydipole@pku.edu.cn

†Electronic address: guenterg@desy.de

‡Electronic address: daniel.britzger@desy.de

§Electronic address: roman.kogler@desy.de

Contents

I. Introduction	4
II. Theoretical Framework	5
A. Renormalisation	6
B. Running coupling and Asymptotic Freedom	6
C. Parton Distribution Function	6
D. Neutral Current Deep Inelastic Scattering Process at HERA	7
E. The Factorisation Theorem	8
F. Jet production	8
III. Cross Section Calculation and Fitting Techniques	9
A. NLO jet cross section	9
B. FastNLO	10
C. Fitting techniques	11
1. χ^2 definition	11
2. Fitting with Minuit	11
IV. α_s extraction from ZEUS Inclusive-jet and Dijet data	12
A. Inclusive-Jet	12
B. Dijet	12
V. Renormalisation Scale, Factorisation Scale and PDF dependence of Cross Section and α_s	15
A. μ_R dependence	16
B. μ_F dependence	17
C. PDF dependence and PDF errors	17
1. PDF dependence of the result	17
2. PDF error determination	20
VI. Conclusion	21
Acknowledgments	24

I. INTRODUCTION

Quantum Chromodynamics (QCD) is a theoretical framework which describes strong interaction, one of the four fundamental forces in nature. It describes the interaction between quarks and gluons, and in particular how they bind together to form hadrons, of which the proton is the most familiar example. QCD emerged as a mathematically consistent theory in the 1970s with the discovery of colour confinement and asymptotic freedom. Nowadays, it is regarded as one of a cornerstone of the extremely successful Standard Model (SM) of elementary particles and their interactions.

Since the discovery of SM, a great number of experiments have been designed to perform precise test of the validity of SM and search for physics beyond at highest available centre of mass energy and luminosity. In the past several decades, the e^+e^- collider LEP (Large Electron Positron Collider) at CERN, the $p\bar{p}$ collider Tevatron at FermiLab and the ep collider HERA (Hadron-Elektron-Ring-Anlage) at DESY, together with other experiments in the same period, laid several milestones in discovering all elementary particles predicted by the SM but Higgs Boson [1]. With the advent of Large Hadron Collider (LHC) at CERN, pp collisions with unprecedented centre-of-mass energies and luminosity become available, allowing the mass production of particles with masses of a few TeV, which greatly enlarges the possibility that people discover new particles predicted by both SM and especially SUSY. However, in order to claim the discovery of new phenomena at the LHC, a precise understanding of SM is indispensable. This includes a precise knowledge in particular of the strong interaction, including the largest part of the pp cross section, of the running of the strong coupling constant α_s and of the internal structure of the protons, which is parametrised by Parton Distribution Functions (PDFs). [2]

The study of jet production in deep inelastic scattering (DIS) at HERA has been well established as a testing ground of perturbative QCD (pQCD), providing large amount of data for extracting the value of strong coupling $\alpha_s(M_Z)$, testing the running of α_s and comparing different sets of PDFs. A large amount of work has been done to extract α_s and PDF from data collected at HERA [3–8] and many other experiments. However, these analysis usually make different choices of renormalisation scale, which makes the comparison of the result between different analysis not as convincing as the comparison on the same analysis basis. To compare the result with the same choice of scale will improve our knowledge of α_s and

PDF to some extent.

Moreover, in the framework of QCD quarks and gluons carry color charge, which comes in three flavours and described by a $SU(3)$ gauge theory. The relative strength of interactions between colored particles is governed by the strong coupling constant α_s , which decreases with increasing energy. Running of α_s [9] can be predicted within QCD, but its value at some starting scale is not predictable in the framework of SM and needs to be extracted from experimental data. The smallness of α_s at high energies leads to an asymptotically free theory, allowing for perturbative methods to be applicable. However, at small enough energies the value of α_s becomes large. In this energy regime, QCD is believed to exhibit the property of confinement, such that colored particles cannot be observed as free states but are confined in colorless bound states, called hadrons. In this case, perturbative methods are not applicable and therefore the structure of hadrons, most importantly the proton PDFs, can only be determined either experimentally or using lattice method.

The uncertainties from the determination of the proton PDFs and α_s would translate into uncertainties of SM predictions in important discovery channels for Higgs searches and searches for new phenomena at the LHC. Thus, a careful analysis of the validity of the running of α_s and the factorisation theorem with the data at hand is also of vital importance.

In this analysis, I managed to extract α_s from both Inclusive-jet and Dijet data, focusing on the study of α_s dependence on the renormalisation scale (μ_R), the factorisation scale (μ_F) and PDF based on data collected by the ZEUS experiment during the HERA-II running in the years 2003-2007 [10, 11]. The report is organized as follows: In Sec. II, the theoretical frame work of QCD, DIS and jet production is provided. In Sec. III, the cross section calculation method is introduced. In Sec. IV, the result of the strong coupling constant α_s and the relative errors is discussed. In Sec. V, the cross section and α_s dependence on μ_R and PDF is shown and illustrated. Sec. VI gives a summary of the results.

II. THEORETICAL FRAMEWORK

QCD is a theory that describes the interaction between quarks and gluons. The main feature of the theory is displayed below. [12]

A. Renormalisation

A crucial requirement of any field theory is renormalisability, which allows us to make physical predictions. Renormalisation can be understood as the replacement of the bare charge and the bare coupling by some physically observed quantities to get rid of the ultraviolet (UV) divergences. This requires the introduction of one new mass scale μ_R in the theory, which defines the point at which the subtractions which remove the UV divergences are performed. Though the result of any physical quantity are the same when summing over all loop contributions, the result of any finite order calculation have a dependence on this scale μ_R .

Considering the fact that the result of any physical observable should not depend on the scale μ_R , we demand the Renormalisation Group Equation (RGE),

$$\left(\mu_R \frac{\partial}{\partial \mu_R} + \beta(\alpha_s) \frac{\partial}{\partial \alpha_s} \right) \Gamma(p_i, \alpha_s) = 0, \quad (1)$$

where $\beta(\alpha_s) = \mu_R \frac{\partial \alpha_s}{\partial \mu_R}$.

B. Running coupling and Asymptotic Freedom

With the RGE, we can determine the α_s dependence on μ_R up to four loops, which enables us to calculate μ_R for any arbitrary scale from a fixed starting scale, which is usually the energy scale of M_Z and the value of α_s for this typical scale $\alpha_s(M_Z)$. For one loop solution,

$$\alpha_s(\mu_R) = \frac{\alpha_s(M_Z)}{1 + \frac{\beta_0}{4\pi} \alpha_s(M_Z) \ln(\mu_R^2/M_Z^2)}, \quad (2)$$

the fact that β_0 is positive, which means α_s decrease with increasing μ_R , making QCD an asymptotic free theory.

C. Parton Distribution Function

In the quark-parton model, the proton is composed of a number of point-like partons (quarks and gluons), while the interaction between leptons and protons in DIS is taken to be the sum of the interaction between the lepton and all the partons in the proton. A parton distribution function (PDF) is defined as the probability density for finding a particle with

a certain longitudinal momentum fraction x at momentum transfer Q^2 . Since pQCD is no longer valid in this case and Lattice QCD has many limitations, PDF is currently determined by using experiment data. In this analysis, we use many sets of PDF and compared the result.

D. Neutral Current Deep Inelastic Scattering Process at HERA

The Neutral Current Deep Inelastic Scattering (NC DIS) process plays an important role in the determination of proton structure and testing the validity of perturbative QCD. The kinematics of DIS is shown in Fig. 1.

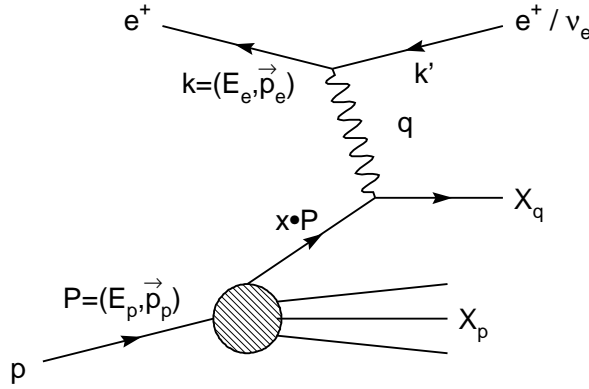


FIG. 1: Kinematics of Deep Inelastic Scattering

The centre-of-mass energy in ep scattering is given by the square root of the Mandelstam variable

$$s = (k + P)^2. \quad (3)$$

where k and P are the four-vectors of the incoming electron and proton, respectively. Assuming massless particles, the centre-of-mass energy at HERA can be well approximated by $\sqrt{s} \approx 4E_e E_p$ where E_e and E_p are the energies of the incoming electron and proton, respectively. The virtuality Q^2 can be calculated from the four-vectors of the incoming and outgoing leptons,

$$Q^2 = -(k - k')^2. \quad (4)$$

The Bjorken scaling variable x can be interpreted in leading order (LO) as the fraction of the momentum of the incoming proton taken by the struck quark, which is,

$$x_{B_j} = \frac{Q^2}{2P \cdot q}. \quad (5)$$

With these four variables, we are able to describe a DIS process kinematically.

E. The Factorisation Theorem

In DIS, the presence of a bound state of partons in the initial state, i.e. the proton inevitably leads to the breakdown of pQCD method below some energy scale μ_f . The factorisation theorem enables us to separated the perturbative and non-perturbative QCD effect by a new mass scale μ_F , the factorisation scale. So we can write down the cross section of DIS in the form of a perturbative serie.

F. Jet production

Jet production in NC DIS provides an ideal environment for studying QCD. While inclusive DIS gives only indirect information on the strong coupling α_s , via the scaling violation, dijet and trijet production allows a direct measurement of α_s . The LO dijet production diagrams are shown in Fig. 2 for QCD Compton and Fig. 3 for Boson-Gluon Fusion.

In LO, the centre-of-mass energy squared of the virtual boson and the incoming parton coincides with the squared invariant mass of the outgoing partons, which is $M_{12}^2 = (p_1 + p_2)^2$. With only kinematics, we can determine the fraction ξ of the proton's momentum carried by the initial state parton ($p_a = \xi P$) to be:

$$\xi = x \left(1 + \frac{M_{12}^2}{Q^2} \right) \quad (6)$$

The jet analysis is performed in the Breit frame where the virtual boson interacts head-on with the proton: $2x_{B_j}\vec{P} + \vec{q} = 0$, where \vec{P} and \vec{q} are the momentum of the proton and the virtual boson, which is completely space-like. In the Breit frame, the Born processes of DIS are processes with zero transverse momentum (p_T) and thus can be easily separated from processes involving strong interaction.

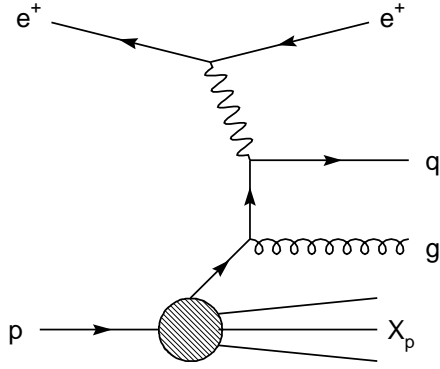


FIG. 2: Dijet Production in NC DIS: QCD Compton

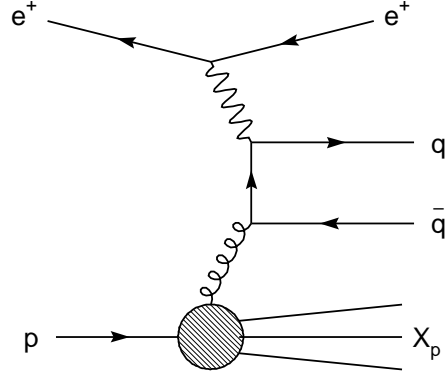


FIG. 3: Dijet Production in NC DIS: Boson Gluon Fusion

III. CROSS SECTION CALCULATION AND FITTING TECHNIQUES

In the QCD fits the free parameters are determined in an iterative minimization procedure of a suitably defined χ^2 function. This requires calculation of cross section to next-to-leading order (NLO) for varying values of $\alpha_s(M_Z)$ and different PDFs. In this analysis, we use “FastNLO” [13, 14] to perform fast calculation of the NLO cross section for the iterative minimization.

A. NLO jet cross section

The DIS cross section is given by

$$\sigma = \sum_{m=1}^{\infty} \sum_a \int_0^1 dx f_a(x, \mu_f) \cdot \Gamma^m(\{p\}_m, x) |\mathcal{M}(p, a_m)|^2 \cdot F^J(p_m), \quad (7)$$

where m is the number of partons in the final state, a runs over all the flavors, x is the fraction of momentum of the parton of flavor a in the proton, f_a is the parton distribution function, $d\Gamma^m$, p_m are the phase space and the set of momenta of the particles m respectively, \mathcal{M} is the matrix element of the partonic process and F^J is the jet function.

During the NLO calculation, three types of divergences appear. An ultraviolet divergence appear in the virtual contribution. This divergence is taken care of by renormalization procedure. Soft and collinear divergences appear in the real and virtual contributions. The first one is compensated between real and virtual contributions and the second one is

absorbed in the parton distribution function. The complex structure of these singularities make the analytical integration in the phase space very difficult, which makes numerical integration almost the only choice.

B. FastNLO

We can generally write the DIS cross section in Eq. 7 as

$$\sigma = \sum_{a,n} \int_0^1 dx c_{a,n} \left(\frac{x_{B_j}}{x}, \mu_R, \mu_F \right) \cdot [\alpha_s^n(\mu_R) \cdot f_{a/h}(x, \mu_F)], \quad (8)$$

a series expansion in terms of α_s with some coefficient $c_{a,n} \left(\frac{x_{B_j}}{x}, \mu_R, \mu_F \right)$.

The basic idea of the FastNLO method is to rewrite Eq. 8 into a factorizable expansion where the convolution of the perturbative coefficient and the partonic functions are reduced to a product.

In order to achieve this, the integral over x should be replaced by summing up discrete number of $x^{(k)}$. Consequently, $\alpha_s^n(\mu_R) \cdot f_{a/h}(x, \mu_F)$ in Eq. 8 is approximated by

$$\sum_{k,l,m} \alpha_s^n(\mu_R^{(l)}) \cdot f_{a/h}(x^{(k)}, \mu_F^{(m)}) \cdot e^{(k)}(x) \cdot b^{(l)}(\mu_R) \cdot d^{(m)}(\mu_F), \quad (9)$$

where $e(x), b(\mu_R), d(\mu_F)$ are interpolation functions. Inserting Eq. 9 in Eq. 8,

$$\sigma = \sum_{a,n,l,k,m} \tilde{\sigma}_{n,a,k,l,m} \alpha_s^n(\mu_R^{(l)}) f_{a/h}(x^{(k)}, \mu_F^{(l)}), \quad (10)$$

where

$$\tilde{\sigma}_{n,a,k,l,m} = c_{a,n} \left(\frac{x_{B_j}}{x}, \mu_R, \mu_F \right) \cdot [e^{(k)}(x) \cdot b^{(l)}(\mu_R) \cdot d^{(m)}(\mu_F)]. \quad (11)$$

The FastNLO concept provides computer code and tables of pre-computed perturbative coefficients generated by NLOjet++ [13, 14], which allows very fast computation of the jet cross section for arbitrary PDFs and $\alpha_s(M_Z)$. Tables and corresponding user-code are available on the FastNLO web sites for a large number of data-sets.

In the present work, we use ZeusDesy10170Dijets_10x10x500M.tables.tab for dijet analysis and ZeusIncJets_0608048_50G.tab for inclusive jet analysis. The factorization scale is chosen to be Q^2 while the renormalisation scale are set to be both Q^2, P_T^2 and $\frac{Q^2 + P_T^2}{2}$. A comparison between the result of choices of distinct renormalisation scale is performed which is shown in Sec. V A. The double differential cross section $d^2\sigma_{jet}/dQ^2 dE_T$ for 22 bins for dijet and 30 bins for inclusive-jet [10, 11], measured by ZEUS collaboration, are calculated with FastNLO using 5 sets of PDFs and the α_s fit result is compared in Sec. V C.

C. Fitting techniques

The fit of α_s is performed in a χ^2 minimization using the program TMinuit of the Root framework, where the definition of χ^2 takes into account all correlations of experimental and theoretical uncertainties.

1. χ^2 definition

In our work we will consider the following definition of the χ^2 ,

$$\chi^2(\alpha_s, \vec{\epsilon}) = \sum_i \frac{(\sigma_i^{exp} - \sigma_i^{the}(\alpha_s)[1 - \sum_k \delta_{i,k}(\epsilon_k)])^2}{\delta_{i,uncorr}^2} + \sum_k \epsilon_k^2, \quad (12)$$

where the index i runs over all bins of Q^2 and P_T that is under analysis, σ_i^{exp} is the experimental cross section, $\sigma_i^{the}(\alpha_s) = \sigma_i^{FastNLO}(\alpha_s) \otimes [C_{Z^0} \cdot C_{Had}]$ is determined from the cross section calculated by FastNLO and the Z^0 and the hadronization corrections provided by the ZEUS Collaboration, k runs over all sources of correlated errors, $\delta_{i,k}$ is the contribution from the k -th correlated error source of the i -th measurement from certain ϵ_k , $\delta_{i,uncorr}$ is the uncorrelated uncertainty, including only the statistical uncertainty in this analysis, the gaussian random variable ϵ_k correspond to the k -th correlated errors and are allowed to be free in the fitting.

In the present analysis, the correlated uncertainties are systematic uncertainty and energy scale uncertainty and the uncorrelated error is only the statistical uncertainty as provided by the ZEUS Collaboration.

2. Fitting with Minuit

Minuit is a collection of minimization libraries developed for finding the minimum value of a multi-parameter function and analyze the shape of the function around the minimum. The basic concept of minuit is that it acts on a multi-parameter function called FCN, which calculates the χ^2 between the prediction and the data. In the present work, the free parameters of FCN are the α_s and ϵ_k .

IV. α_s EXTRACTION FROM ZEUS INCLUSIVE-JET AND DIJET DATA

The value of the strong coupling constant is a function of the renormalization scale μ_R which is shown in Sec. II A and Sec. II B. The value of α_s at any scale can be calculated from the value at a specific scale with the RGE. Usually, this scale is chosen to be the Z^0 boson mass $M_Z = 91.1876\text{GeV}$. The perturbative QCD prediction of the inclusive jet and dijet production cross sections are calculated with the updated version of the FastNLO package, where the renormalization scale μ_R can be set by hand. The analysis is performed in Breit frame, and the uncorrelated and correlated errors are treated carefully. A wide range of proton PDFs are used in the analysis and the results are shown separately in both inclusive and dijet production analysis.

A. Inclusive-Jet

The present analysis of ZEUS Inclusive-Jet data is based on the published data shown in Table 8 of reference [10]. We fitted α_s with 5 families of PDFs and 3 choices of renormalisation scale, taking into account only the detector systematic uncertainty but not the luminosity uncertainty, the energy scale uncertainty. The results for α_s for all bins and for bins with $Q^2 > 500\text{GeV}^2$ only are shown in Table. IV A and Fig. 4.

The published result of the ZEUS Collaboration is

$$\alpha_s(M_Z) = 0.1207 \pm 0.0014(stat.)_{-0.0033}^{+0.0035}(exp.)_{-0.0023}^{+0.0022}(th.), \quad (13)$$

with the NLO calculations based on the ZEUS-S PDFs. The result of α_s obtained in our analysis with CTEQ6.6 and CTEQ6m is consistent within 1% with the published result, as is proposed by the ZEUS Collaboration. However, the α_s obtained by NNPDF2.1_100 is a little smaller than the published value. Moreover, in the analysis, we also observe an α_s dependence on the renormalisation scale and factorisation scale we choose. This μ_R and μ_F dependence will also be studied in more detail with the dijet fit result.

B. Dijet

The present analysis of ZEUS Dijet data is based on the published data shown in Table 8 of reference [11]. α_s is fitted with 5 families of PDFs, 3 choice of μ_R and μ_F . The results

μ_F^2	μ_R^2	PDFs	Bin	α_s	err(stat)	χ^2/ndf
Q^2	E_T^2	cteq6m	All	0.12175	0.00095	1.29404
Q^2	E_T^2	CT10	All	0.12187	0.00086	1.33967
Q^2	E_T^2	CTEQ6.6	All	0.12231	0.00085	1.33006
Q^2	E_T^2	MSTW2008	All	0.12208	0.00108	1.48301
Q^2	E_T^2	HERAPDF1.0	All	0.11956	0.0005	1.52181
Q^2	E_T^2	cteq6m	$Q^2 > 500$	0.1220	0.0021	1.3559
Q^2	E_T^2	HERAPDF1.0	$Q^2 > 500$	0.1185	0.0020	1.5687
Q^2	E_T^2	CTEQ6.6	$Q^2 > 500$	0.1221	0.0021	1.3955
Q^2	E_T^2	CT10	$Q^2 > 500$	0.1215	0.0021	1.3896
Q^2	E_T^2	HERAPDF1.5	$Q^2 > 500$	0.1186	0.0020	1.5538
Q^2	E_T^2	MSTW2008	$Q^2 > 500$	0.1210	0.0021	1.3856
Q^2	E_T^2	NNPDF2.1_100	$Q^2 > 500$	0.1197	0.0022	1.3895

TABLE I: Inclusive-Jet α_s fit result for both all 30 bins and bins with $Q^2 > 500$ with different PDFs

are shown in Table. III,IV and V and selected result are shown in Fig. 5.

The value of α_s is obtained from the measured $d\sigma/dQ^2 dP_T$ for all 22 bins by the ZEUS Collaboration [11] using the PDFs family CTEQ6.6 with a choice of renormalisation scale of $(Q^2 + E_T^2)/2$,

$$\alpha_s(M_Z) = 0.1173 \pm 0.0026(stat.)^{+0.0009}_{-0.0002}(PDF)^{+0.0103}_{-0.0097}(th.), \quad (14)$$

This value of $\alpha_s(M_Z)$ in Eq. 14 is consistent with the current world average of $\alpha_s(M_Z) = 0.1184 \pm 0.0007$ [16] and the H1 result [19]. As a cross check, $\alpha_s(M_Z)$ is determined by calculation with four more family of PDFs. The values obtained with CT10, CTEQ6m and HERAPDF1.5 are consistant within 1% with those based on CTEQ6.6, while the result obtained with NNPDF2.1 is much smaller than the value obtained by the rest, as is shown in Table. VI.

We calculated the Thoery-over-Data Cross Section Ratio for the best fit α_s value with four different PDFs (CTEQ6.6, CT10, HERAPDF1.5 and NNPDF2.1_100), which is shown

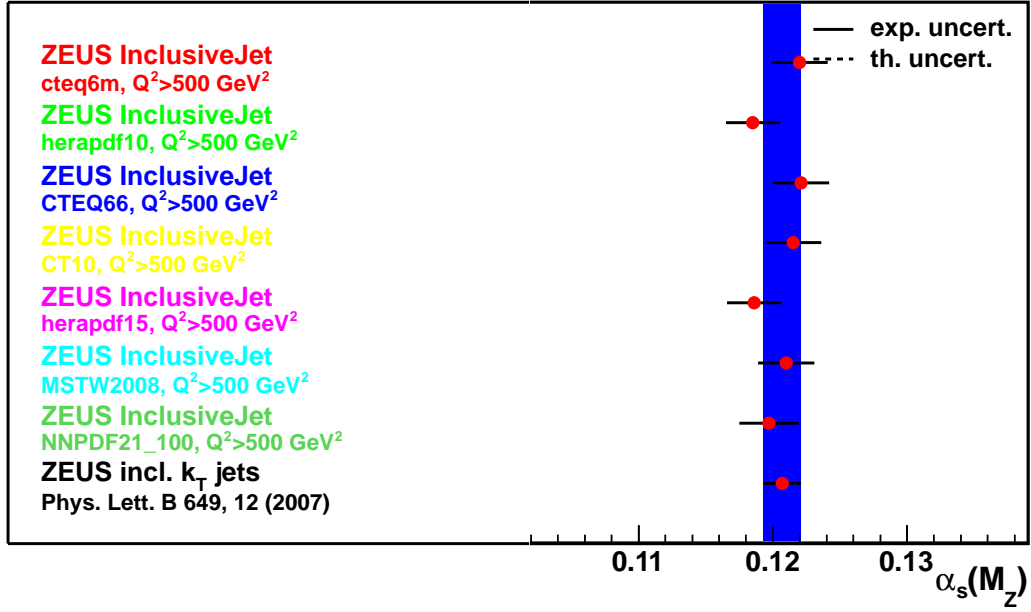


FIG. 4: The Inclusive-Jet α_s fit result with different PDFs

in Fig. 6

In this Figure, the error of data is shown with black error bar around the central value 1, which is just the experimental cross section. The data is shown with four different colors for four different PDFs with which we calculated the cross section for the best fit α_s value and the light blue error bar is the theoretical error for CTEQ6.6. We can see from Fig. 6 that the difference between theory and data is small for most bins. However, for the high Q^2 high P_T bins, a 5% larger theoretical cross section is observed, which agrees with the result of the fit for each bin individually of the Dijet data. The result of the fit for each bin individually is shown in Fig. 7. From this figure, we can see that the result agrees with prediction very well for the low Q^2 and low P_T bins. However, for high Q^2 high P_T bins, there is a larger difference which agrees with the result in Fig. 6.

Further, we studied the asymptotic free feature of QCD with the α_s value we obtained from the fit, the running of α_s feature agrees with theoretical prediction very well in $5 < Q < 50$ GeV region, which is shown in Fig. 8. In this figure, the shadow area is the α_s value from global fit, while the pink points are the result of α_s fit for each bin shown at the corresponding μ_R .

μ_F^2	μ_R^2	PDFs	Bin	α_s	err(stat)	χ^2/ndf
Q^2	E_T^2	CTEQ6m	All	0.12175	0.00095	1.29404
$2Q^2$	E_T^2	CTEQ6m	All	0.12164	0.00079	1.30668
$(Q/2)^2$	E_T^2	CTEQ6m	All	0.12214	0.00172	1.37733
Q^2	$(2E_T)^2$	CTEQ6m	All	0.12664	0.00085	1.50757
Q^2	$(E_T/2)^2$	CTEQ6m	All	0.12454	0.0019	1.69201
$Q^2/2$	$(E_T/2)^2$	CTEQ6m	All	0.12446	0.00178	1.85459
$(2Q)^2$	$(2E_T)^2$	CTEQ6m	All	0.12643	0.00085	1.62312
Q^2	$Q^2 + E_T^2$	CTEQ6m	All	0.12672	0.00187	1.30504
Q^2	$(Q^2 + E_T^2)/2$	CTEQ6m	All	0.12486	0.00184	1.31517
Q^2	$(Q^2 + E_T^2)/4$	CTEQ6m	All	0.12358	0.0018	1.34941

TABLE II: Inclusive-Jet α_S fit result for all 30 bins with different choices of μ_R and μ_F

μ_F^2	μ_R^2	PDFs	α_s	err(stat)	χ^2/ndf
Q^2	E_T^2	cteq6m	0.1079	0.0017	4.206
Q^2	E_T^2	CT10	0.1082	0.0017	3.962
Q^2	E_T^2	CTEQ6.6	0.1085	0.0017	4.075
Q^2	E_T^2	HERAPDF1.5	0.1078	0.0019	2.931
Q^2	E_T^2	NNPDF2.1_100	0.1065	0.0017	3.744

TABLE III: Dijet α_S fit result for different PDFs with $\mu_R^2 = E_T^2$

V. RENORMALISATION SCALE, FACTORISATION SCALE AND PDF DEPENDENCE OF CROSS SECTION AND α_s

In this section, a detailed analysis of the dependence of the result of α_s on the choices of the renormalisation scale μ_R , the factorization scale μ_F and the PDFs is presented.

μ_F^2	μ_R^2	PDFs	α_s	err(stat)	χ^2/ndf
Q^2	Q^2	cteq6m	0.1163	0.0026	1.350
Q^2	Q^2	CT10	0.1168	0.0026	1.326
Q^2	Q^2	CTEQ6.6	0.1163	0.0025	1.292
Q^2	Q^2	HERAPDF1.5	0.1155	0.0027	1.317
Q^2	Q^2	NNPDF2.1_100	0.1132	0.0024	1.389

TABLE IV: Dijet α_s fit result for different PDFs with $\mu_R^2 = Q^2$

μ_F^2	μ_R^2	PDFs	α_s	err(stat)	χ^2/ndf
Q^2	$(Q^2 + E_T^2)/2$	cteq6m	0.1168	0.0026	1.333
Q^2	$(Q^2 + E_T^2)/2$	CTEQ6.6	0.1173	0.0026	1.288
Q^2	$(Q^2 + E_T^2)/2$	CT10	0.1168	0.0026	1.257
Q^2	$(Q^2 + E_T^2)/2$	HERAPDF1.5	0.1162	0.0028	1.212
Q^2	$(Q^2 + E_T^2)/2$	NNPDF2.1_100	0.1137	0.0024	1.309

TABLE V: Dijet α_s fit result for different PDFs with $\mu_R^2 = (Q^2 + E_T^2)/2$

A. μ_R dependence

The renormalisation scale μ_R dependence of α_s fitting result is determined for CTEQ6.6, CTEQ6m CT10, HERAPDF1.5 and NNPDF2.1. The selected results are shown in III, IV and V for three kinds of choices of μ_R . The result of the α_s fit with a choice of renormalisation scale $\mu_R^2 = P_T^2$ is not as preferred as the result obtained with $\mu_R^2 = Q^2$ and $\mu_R^2 = (Q^2 + P_T^2)/2$.

To figure out the reason for this inconsistency, we calculate the cross section for each bin of Q^2 P_T from $\mu_R/2$ to $2\mu_R$ with different μ_R choices. The result of $\mu_R^2 = P_T^2$ and $\mu_R^2 = (Q^2 + P_T^2)/2$ are shown in Fig. 12 and Fig. 13 for comparison.

From the comparison between Fig. 12 and Fig. 13, we can easily find that for low P_T , high Q^2 bins, the cross section drops unexpectedly fast when we scale μ_R to be $\mu_R/2$, which is shown more clearly in Fig. 9 and Fig. 10. Such unexpected drop is caused by the break down of pQCD calculation at low scale, which generate a big theoretical error in the calculation with $\mu_R = P_T^2$. However, with $\mu_R^2 = (Q^2 + P_T^2)/2$ especially and also $\mu_R^2 = Q^2$, the

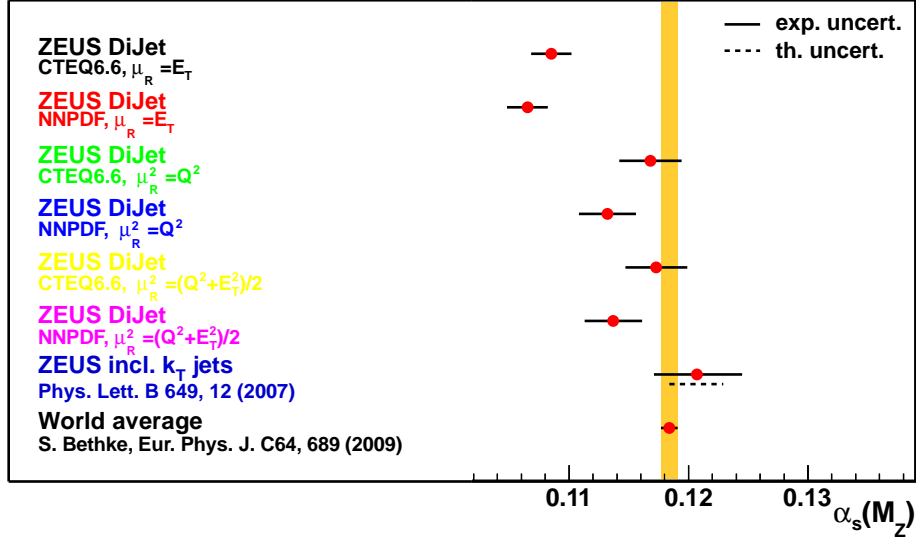


FIG. 5: Selected Dijet α_s fit result

perturbative property is safely preserved for both low P_T and low Q^2 region. The theoretical uncertainty due to μ_R for CTEQ6.6 is determined to be $^{+0.01018}_{-0.00966}$ on α_s .

B. μ_F dependence

The NLO cross section calculation result dependence on the factorisation scale μ_F is not as strong as the dependence on the renormalisation scale μ_R . We also calculated the cross section dependence on μ_F and the cross section behaves generally well with both $\mu_F^2 = P_T^2, \mu_F^2 = Q^2$ and $\mu_F^2 = (Q^2 + P_T^2)/2$ as expected. The α_s fit result are in consistent within 1% for both CTEQ6.6 and NNPDF2.1_100, and the theoretical uncertainty due to factorisation scale μ_F for CTEQ6.6 is determined to be $^{+0.00212}_{-0.00185}$ on α_s .

C. PDF dependence and PDF errors

1. PDF dependence of the result

The PDF dependence of the α_s result is determined with $\mu_R^2 = (Q^2 + P_T^2)/2$ and $\mu_F^2 = Q^2$ and the selected result is shown in Fig. VI.

From Table VI, it is clear that the α_s fit result for CTEQ6.6, CT10 and HERAPDF1.5

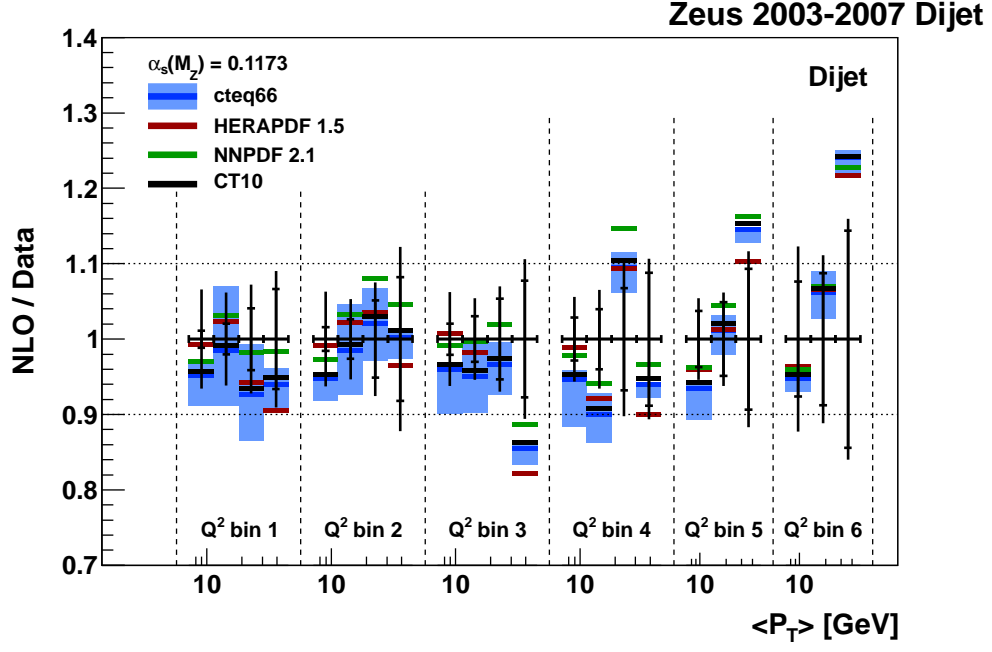


FIG. 6: Theory-over-Data Ratio for the best fit α_s value

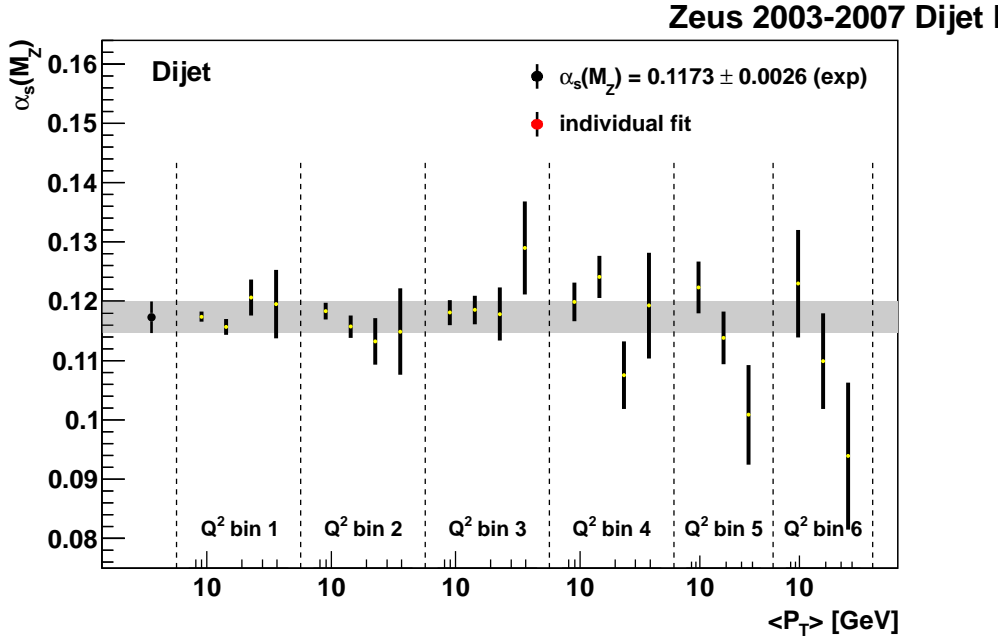


FIG. 7: $\alpha_s(M_Z)$ Fit Result for Each Bin with Dijet data

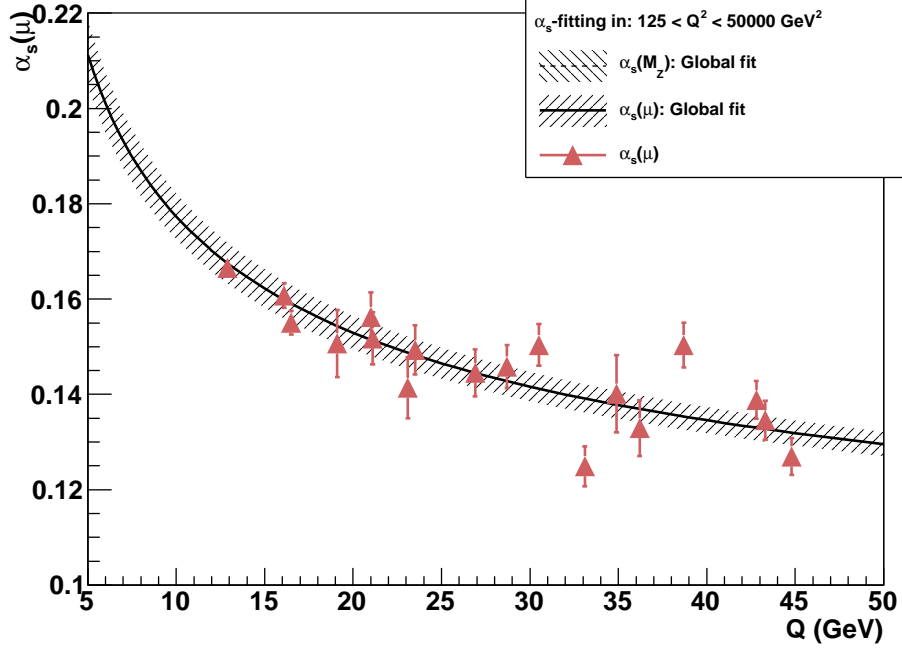


FIG. 8: Running α_s property from α_s fitted for each bin

μ_F μ_R	PDFs	α_s	err(stat)	χ^2/ndf
Q^2 $(Q^2 + E_T^2)/2$	CTEQ66	0.1173	0.0026	1.288
Q^2 $(Q^2 + E_T^2)/2$	CT10	0.1168	0.0026	1.257
Q^2 $(Q^2 + E_T^2)/2$	HERAPDF1.5	0.1162	0.0028	1.212
Q^2 $(Q^2 + E_T^2)/2$	NNPDF2.1_100	0.1137	0.0024	1.309

TABLE VI: Selected Dijet α_s fit result with different PDF choice

is generally consistent with each other, while the result of NNPDF2.1_100 is smaller by 3%. This could come from the fact that NNPDF uses a conceptually different method, the neural network approach [17]. Basically, the approach of CTEQ6.6 and CT10 are similar, people first choose a function form with certain number of free parameters ($22 \sim 26$ for CTEQ), evolve the function to some desired scales and compute the physical observables for these scales. After comparing the computed physical observables with experimental data, the best-fit value of parameters is determined and the PDF error is determined by propagation of error on parameters, which is quite similar with the α_s fit approach in the present work.

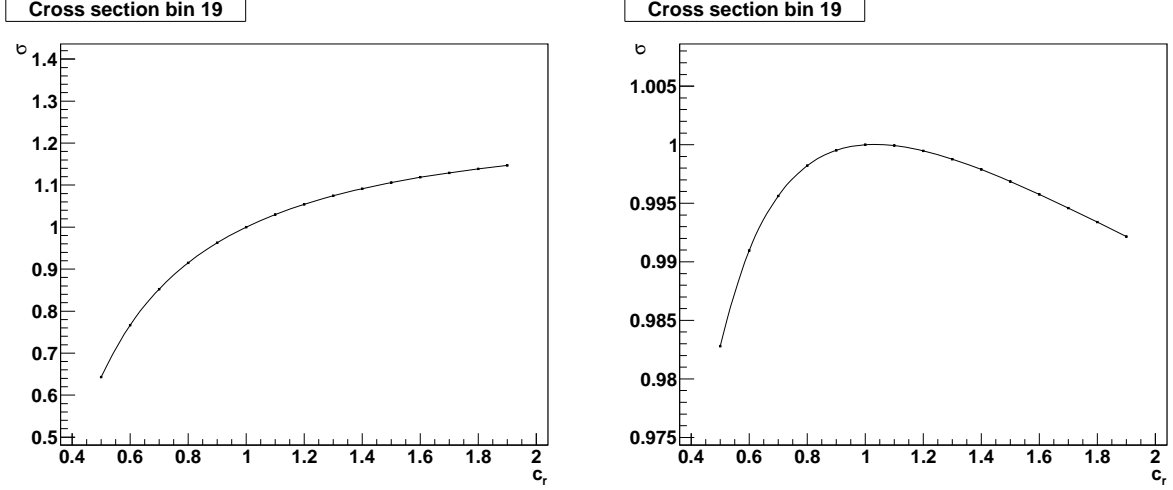


FIG. 9: $\mu_R = P_T^2$ Bin 19: $P_T(8 \sim 16)GeV$, $Q^2(5000 \sim 20000)GeV^2$ FIG. 10: $\mu_R^2 = (Q^2 + P_T^2)/2$ Bin 19: $P_T(8 \sim 16)GeV$, $Q^2(5000 \sim 20000)GeV^2$

However, for NNPDF, the determination of PDFs is done by the monte carlo sampling of the probability measure in the fuction space of PDFs. The determination of PDFs starts from monte carlo sampling of data space. Each PDF is described by a neural network parameterized by 37 parameters, which is large compared to CTEQ6.6. The large number of parameters make NNPDF able to represent any function. The sampled data gives hint to the computer which bins are more populated and the computers are trained to best fit the data. The process stops when the quality of fit to randomly selected data stops improving and the NNPDF people show that overlearning (a fit with χ^2 lower than the best fit) is able to be obtained with this method. The CTEQ kind of PDFs and NNPDF PDFs are different mainly in the low x region for gluon and total strangeness.

However, we are basically not sure why this small value from NNPDF2.1.100 comes about, it requires more study in the future.

2. PDF error determination

The PDF error is determined with three different approaches.

- Fit α_s for all the PDFs contained in a PDF set and use the largest and smallest value of all the eigenvalues respectively to be the up and down error

- Use the PDF Eignvektorer method, in which the shift on the cross section arises from the pdf error.
- Following the master formula introduced in [18]

In the present analysis, we calculated the PDF uncertainty of α_s fit for CTEQ6.6 and NNPDF2.1_100 and compared the result of PDF uncertainty, which is shown as follows.

The largest and smallest shift for all sets:

$$\begin{aligned}\text{CTEQ6.6} : \alpha_s(M_Z) &= 0.1173^{+0.0012}_{-0.0009}(PDF), \\ \text{NNPDF2.1_100} : \alpha_s(M_Z) &= 0.1137^{+0.0051}_{-0.0026}(PDF),\end{aligned}$$

PDF Eignvektorer method(Only valid for CTEQ6.6 at present):

$$\text{CTEQ6.6} : \alpha_s(M_Z) = 0.1173^{+0.0009}_{-0.0002}(PDF), \quad (15)$$

Following master formula:

$$\begin{aligned}\text{CTEQ6.6} : \alpha_s(M_Z) &= 0.1173^{+0.0005}_{-0.0003}(PDF), \\ \text{NNPDF2.1_100} : \alpha_s(M_Z) &= 0.1137^{+0.0013}_{-0.0009}(PDF),\end{aligned}$$

We got the expected feature that the PDF uncertainty from NNPDF2.1_100 is generally larger than that from CTEQ6.6, which basically comes from the larger uncertainty from the PDF itself in low x region. However, we are not sure currently the reason for the small α_s value coming from α_s fit with NNPDFs. We also tried to fit α_s with NNPDF2.1 for different α_s values from $\alpha_s = 0.115$ to $\alpha_s = 0.122$. However, no big difference in the α_s fit result is observed. Therefore, more analysis should be done to understand this property better.

VI. CONCLUSION

In this work, I calculated the cross section of both inclusive and dijet production to NLO based on both the original and updated version of “FastNLO”. α_s is determined from both Inclusive-Jet and Dijet data collected by ZEUS Collaboration from 2003-2007 during the HERA-II run with different choices of parton distribution functions, renormalisation scale, factorisation scale and also a study of the PDF error is performed.

With the Inclusive-Jet data, I managed to fit the strong coupling constant from experimental data with $Q^2 > 500 \text{GeV}^2$ and imposing a choice of μ_F and μ_R which is same with the ZEUS Collaboration [10], I successfully determined α_s to be consistent with the published result. The dependence of this result on the choice of μ_F and μ_R is studied and the reason for a choice of only using bins with $Q^2 > 500 \text{GeV}^2$ for the fit is shown by comparison of the α_s fit result. However, no hint of breakdown of pQCD calculation is observed in the study of the cross section dependence on the scaling of both μ_F and μ_R .

In the Dijet case, the α_s is determined with $\mu_F^2 = Q^2$, $\mu_R^2 = (Q^2 + P_T^2)/2$ and CTEQ6.6 as the PDFs to be

$$\alpha_s(M_Z) = 0.1173 \pm 0.0026(\text{stat.})_{-0.0002}^{+0.0009}(\text{PDF})_{-0.0097}^{+0.0103}(\text{theo}), \quad (16)$$

which is consistent with the current world average of $\alpha_s(M_Z) = 0.1184 \pm 0.0007$ [16] and the HERA average of $\alpha_s(M_Z) = 0.1198 \pm 0.0032$ [16]. As a cross check, $\alpha_s(M_Z)$ is determined by calculation with four more PDF sets. The values obtained with CT10, CTEQ6m and HERAPDF1.5 are consistent within 1% with the value with CTEQ6.6, while the result obtained with NNPDF2.1 is much smaller than the value obtained by the others, as is shown in Table. VI. The theoretical error is determined by considering the variation of μ_R and μ_F .

Moreover, the α_s dependence on the choice of renormalisation scale, factorisation scale and PDFs are studied in detail. It is shown that $\mu_R^2 = P_T^2$ is no longer a good choice for dijet data because of the breakdown of perturbative method in low P_T region while any of the three popular choices of scales are generally valid for μ_F . The discrepancy between NNPDF2.1_100 and CTEQ-like PDF sets is shown. This discrepancy could be a result of the differences of these two family of PDFs in the low x region for gluon and total strangeness, which is due to the difference of the method in determining the PDFs. However, more analysis still need to be done to really figure out the reason for this strange feature. The PDF uncertainty is calculated in three general way and the result is small compared to the theoretical uncertainty due to the choice of μ_R .

We look forward to combining the α_s fit result for ZEUS Inclusive-Jet and Dijet data with the result from H1 experiment published in [19] and producing combined result for α_s fit of HERA. The current status of this analysis is demonstrated in Fig. 11.

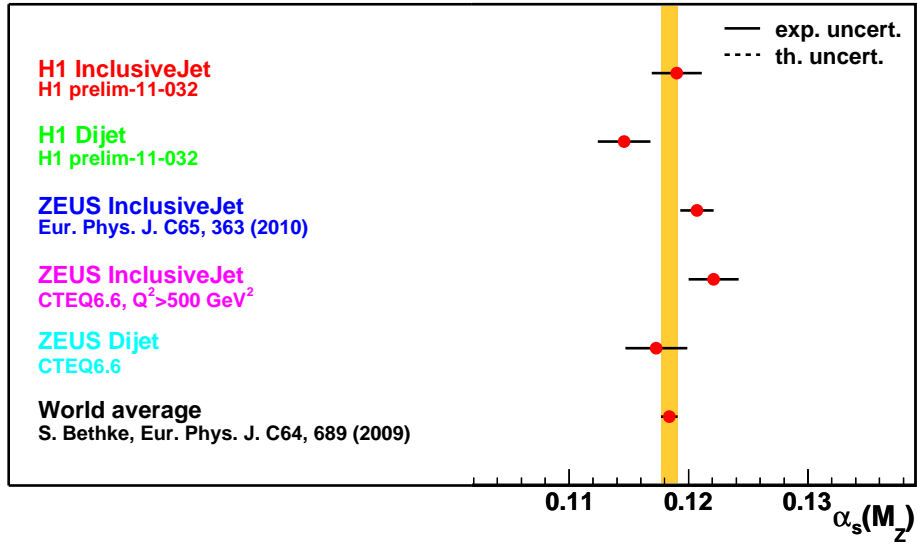


FIG. 11: Combined result of H1 and ZEUS fit result

Acknowledgments

I would like to thank My supervisors Dr. GünterGrindhammer, Daniel Britzger, Dr. Roman Kogler for trusting me and giving me the opportunity to work on this project. I would also like to thank Aziz Dossanov, Luigi, Carlos, Alina, Leonardo, Alex, Edyta and Andrea for their kind assistance and company.

I want to thank Prof. Dr. Olaf Beneke and Mrs. Andrea Schrader, for organizing DESY summer school program 2011 and making my stay at DESY very happy.

-
- [1] R.K. Ellis, W.J.Stirling and B.R. Webber *QCD and Collider Physics* (Cambridge University Press, UK, 2003).
 - [2] M. R. Whalley, D. Bourilkov and R. C. Group, arXiv:hep-ph/0508110.
 - [3] ZEUS Collaboration, J. Breitweg et al., Phys. Lett. B 507 (2001) 70
 - [4] H1 Collaboration, C. Adloff et al., Eur. Phys. J. C 19 (2001) 289
 - [5] ZEUS Collaboration, S. Chekanov et al., Eur. Phys. J. C 23 (2002) 13
 - [6] ZEUS Collaboration, S. Chekanov et al., Nucl. Phys. B 765 (2007) 1
 - [7] ZEUS Collaboration, S. Chekanov et al., Phys. Lett. B 547 (2002) 164
 - [8] ZEUS Collaboration, S. Chekanov et al., Phys. Lett. B 551 (2003) 226
 - [9] D. J. Gross, F. Wilczek, Phys. Rev. Lett. 30 (1973) 1343-1346.
 - [10] S. Chekanov *et al.* [ZEUS Collaboration], Nucl. Phys. B **765** (2007) 1 [arXiv:hep-ex/0608048].
 - [11] H. Abramowicz *et al.* [ZEUS Collaboration], Eur. Phys. J. C **70** (2010) 965 [arXiv:1010.6167 [hep-ex]].
 - [12] R. Kogler, DESY-THESIS-2011-006.
 - [13] Z. Nagy, Phys. Rev. Lett. **88** (2002) 122003 [arXiv:hep-ph/0110315].
 - [14] Z. Nagy, Phys. Rev. D **68** (2003) 094002 [arXiv:hep-ph/0307268].
 - [15] S. Chekanov *et al.* [ZEUS Collaboration], Phys. Lett. B **649** (2007) 12 [arXiv:hep-ex/0701039].
 - [16] S. Bethke, Eur. Phys. J. **C64** (2009) 689-703. [arXiv:0908.1135 [hep-ph]].
 - [17] R. D. Ball, L. Del Debbio, S. Forte, A. Guffanti, J. I. Latorre, J. Rojo, M. Ubiali, Nucl. Phys. **B838** (2010) 136-206. [arXiv:1002.4407 [hep-ph]].
 - [18] J. M. Campbell, J. W. Huston, W. J. Stirling, Rept. Prog. Phys. **70** (2007) 89. [hep-

ph/0611148].

[19] R. Kogler [H1 Collaboration], arXiv:1107.1530 [hep-ex].

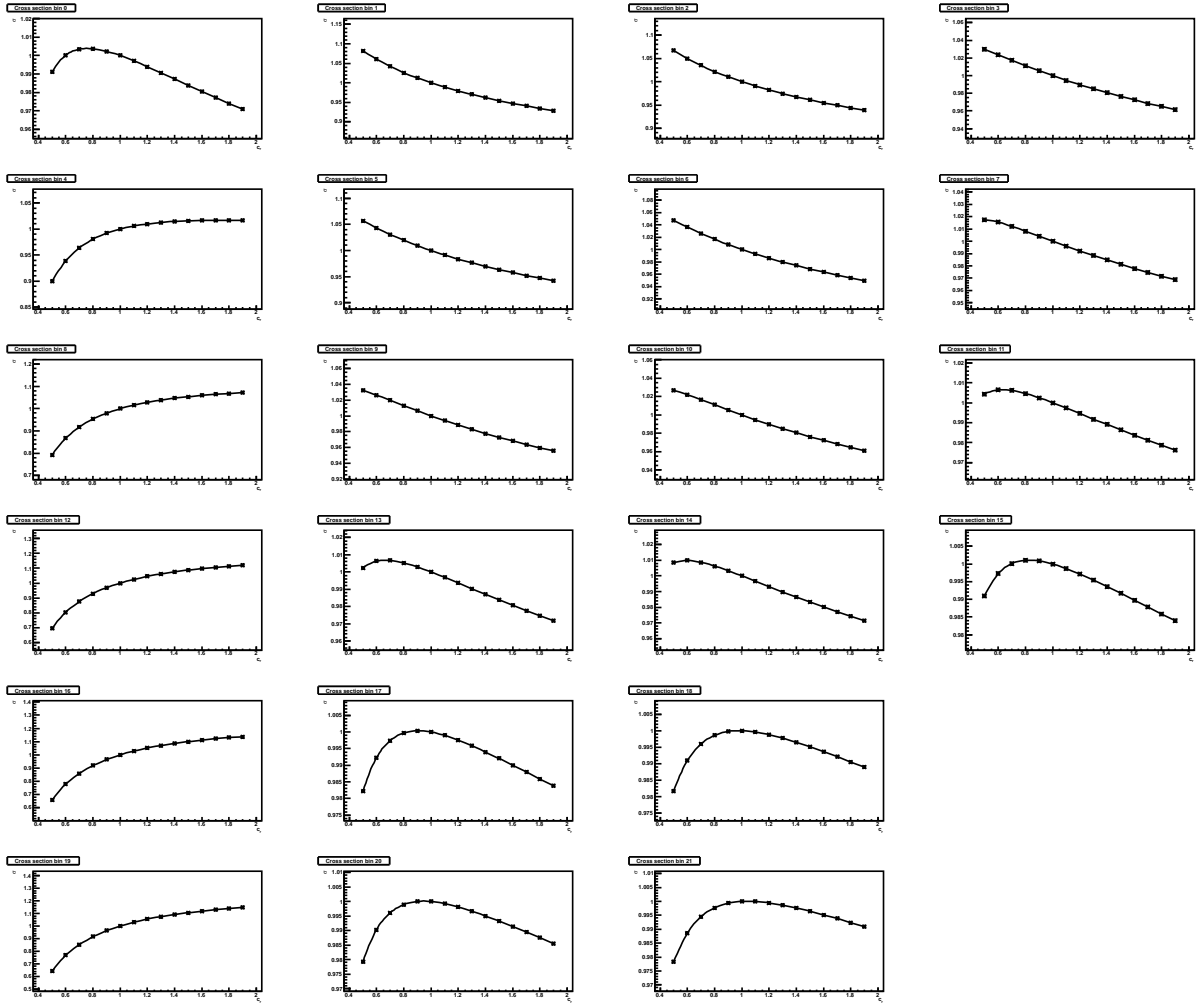


FIG. 12: Dijet Cross Section Evolution with $\mu_R^2 = P_T^2$

E_T bin (GeV)	$d\sigma/dE_T$ (pb/GeV)	δ_{stat}	δ_{syst}	δ_{ES}	C_{QED}	$C_{\text{hadr}} \cdot C_{Z^0}$
$125 < Q^2 < 250 \text{ GeV}^2$						
8 ... 15	5.050	± 0.057	$+0.071$ -0.070	$+0.311$ -0.274	0.97	0.95
15 ... 22	1.385	± 0.028	$+0.037$ -0.038	$+0.063$ -0.062	0.97	0.96
22 ... 30	0.292	± 0.012	$+0.012$ -0.013	$+0.009$ -0.010	0.97	0.96
30 ... 60	0.0241	± 0.0016	$+0.0009$ -0.0008	$+0.0011$ -0.0010	0.97	0.95
$250 < Q^2 < 500 \text{ GeV}^2$						
8 ... 15	2.937	± 0.046	$+0.076$ -0.076	$+0.146$ -0.141	0.95	0.95
15 ... 22	0.998	± 0.026	$+0.011$ -0.011	$+0.040$ -0.035	0.95	0.98
22 ... 30	0.215	± 0.011	$+0.008$ -0.008	$+0.006$ -0.008	0.96	0.97
30 ... 60	0.0195	± 0.0016	$+0.0015$ -0.0015	$+0.0010$ -0.0006	0.93	0.95
$500 < Q^2 < 1000 \text{ GeV}^2$						
8 ... 15	1.502	± 0.031	$+0.055$ -0.054	$+0.064$ -0.052	0.94	0.95
15 ... 22	0.629	± 0.019	$+0.008$ -0.009	$+0.023$ -0.021	0.95	0.99
22 ... 30	0.1665	± 0.0089	$+0.0041$ -0.0041	$+0.0054$ -0.0040	0.96	0.98
30 ... 60	0.0194	± 0.0015	$+0.0010$ -0.0010	$+0.0007$ -0.0010	0.95	0.99
$1000 < Q^2 < 2000 \text{ GeV}^2$						
8 ... 15	0.701	± 0.020	$+0.017$ -0.017	$+0.025$ -0.022	0.93	0.95
15 ... 22	0.352	± 0.014	$+0.012$ -0.013	$+0.011$ -0.009	0.94	1.01
22 ... 30	0.0943	± 0.0064	$+0.0063$ -0.0063	$+0.0025$ -0.0026	0.94	1.02
30 ... 60	0.0136	± 0.0012	$+0.0003$ -0.0004	$+0.0006$ -0.0007	0.94	1.04
$2000 < Q^2 < 5000 \text{ GeV}^2$						
8 ... 16	0.350	± 0.013	$+0.009$ -0.009	$+0.004$ -0.007	0.92	1.00
16 ... 28	0.1191	± 0.0058	$+0.0023$ -0.0022	$+0.0030$ -0.0023	0.93	1.07
28 ... 60	0.01040	± 0.00097	$+0.00053$ -0.00049	$+0.00044$ -0.00046	0.94	1.08
$5000 < Q^2 < 20000 \text{ GeV}^2$						
8 ... 16	0.0995	± 0.0076	$+0.0092$ -0.0092	$+0.0012$ -0.0005	0.93	1.05
16 ... 28	0.0354	± 0.0031	$+0.0023$ -0.0021	$+0.0003$ -0.0008	0.89	1.14
28 ... 60	0.00368	± 0.00053	$+0.00015$ -0.00023	$+0.00016$ -0.00012	0.95	1.20

TABLE VII: Inclusive dijet cross-sections in different regions of Q^2 .

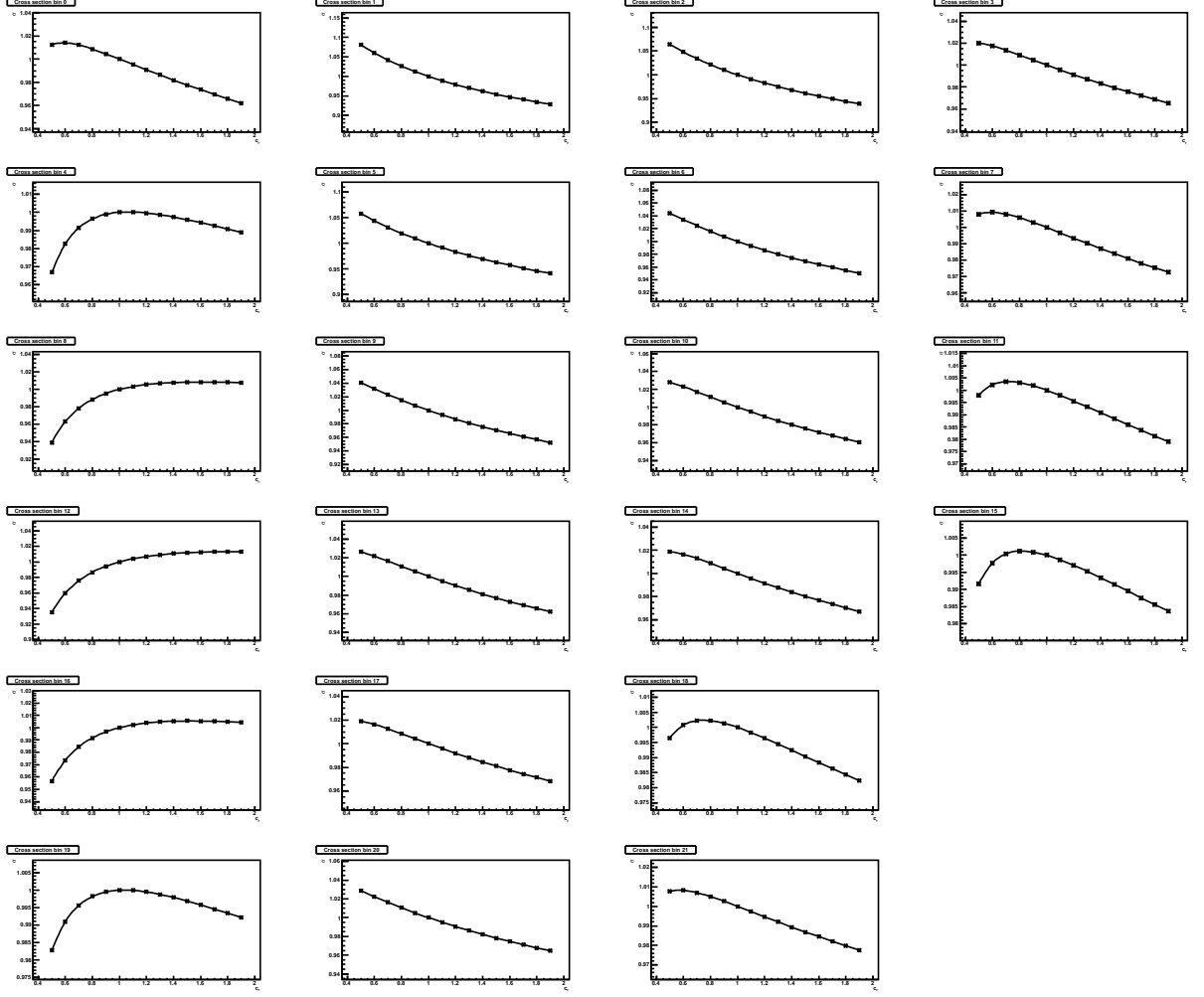


FIG. 13: Dijet Cross Section Evolution with $\mu_R^2 = (Q^2 + P_T^2)/2$